

Quasinormal modes of the Schwarzschild black hole with a deficit solid angle and quintessence-like matter: Improved asymptotic iteration method

L. A. López^{1,*}, Omar Pedraza^{1,†}, Roberto Arceo^{2,‡} and V. E. Ceron^{1,§}

¹ *Área Académica de Matemáticas y Física, UAEH, Carretera Pachuca-Tulancingo Km. 4.5, C. P. 42184, Mineral de la Reforma, Hidalgo, México. and*

² *Facultad de Ciencias en Física y Matemáticas, Universidad Autónoma de Chiapas, C. P. 29050, Tuxtla Gutiérrez, Chiapas, México*

We study the quasinormal modes (QNM) for scalar, and electromagnetic perturbations in the Schwarzschild black hole with a deficit solid angle and quintessence-like matter. Using the sixth-order WKB approximation and the improved asymptotic iteration method (AIM) we can determine the dependence of the quasinormal modes on the parameters of the black hole and the parameters on the test fields. The values of the real part and imaginary parts of the quasi-normal modes increase with the decrease of the values of the deficit solid angle and density of quintessence-like matter. The quasinormal modes gotten by these two methods are in good agreement. Using the finite difference method, we obtain the time evolution profile of such perturbations in this Black Hole.

Keywords: Quasi-normal modes, Quintessence-like matter, WKB approximation, AIM.

PACS numbers: 04.20.-q, 04.70.-s, 04.70.Bw, 04.20.Dw

I. INTRODUCTION

One state resulting from the disturbance (scalar or electromagnetic perturbations) of a black hole (BH) is an oscillation with complex frequencies called quasinormal modes (QNM). The QNM is related to the parameters that describe the BH as mass, charge, angular moment, and others. But also, we can analyze the frequency of oscillation and the damping of the oscillation through the real part and imaginary part of the frequencies of the QNM respectively. Another important contribution of the QNM is the analysis of the stability of the BHs and their gravitational radiation.

The study of QNM has been carried out for different solutions of black holes that represent isolated solutions or in vacuum for example; QNM of Schwarzschild [1], Reissner–Nordström, Hayward [2], and others. Also, different authors have investigated QNM in non-linear electrodynamics (NLED); QNM of Bardeen [3], Einstein-Born-Infeld [4], and Generic-class [5] to mention some investigations.

Now, if we consider that the black holes' coexistence with other types of matter or energy is significant, and according to different observations, dark energy is distributed throughout the universe and is the cause of its expansion. Then, the study of black holes surrounded by dark energy is a topic of current interest.

There are different models as candidates for dark energy and the difference between the models is the magnitude of the state parameter that represents the ratio of pressure to the energy density of dark energy. One of the candidates is the quintessence which differs with the cosmological constant in the magnitude of the state parameter.

The studies of QNM of BHs surrounded by the quintessence have been developed for different scenarios as Hayward [6], Bardeen, Reissner–Nordström [7] and others black holes, all surrounded by quintessence (using the Kiselev model [8]).

In the special case of the Schwarzschild solution, the QNM have been studied in different scenarios considering the influence of dark energy. for example; in [9] and [10] studied the QNM of Schwarzschild surrounded by quintessence, also QNM of a Schwarzschild black hole with a deficit angle and quintessence-like matter are investigated in [11], in [12] studied the QNM of noncommutative Schwarzschild black hole surrounded by quintessence.

In the works above mentioned on the study of QNM, different numerical methods have been applied being the WKB method the most used. When you want to perform the analysis of QNM, this lead to a wave equation with a specific effective potential, depending on the characteristics of the effective potential some numerical methods are more suitable.

*Electronic address: lalopez@uaeh.edu.mx

†Electronic address: omarp@uaeh.edu.mx

‡Electronic address: roberto.arceo@unach.mx

§Electronic address: vceron@uaeh.edu.mx

The asymptotic iteration method (AIM) proposed in [13] to obtain the eigenvalues and eigenfunctions of linear differential equations second-order homogeneous, has shown a method can be a technique efficient and accurate in calculating the frequencies of QNM for a wide variety of black holes, for example in [14] the QNM of Schwarzschild, Schwarzschild anti-de Sitter or de Sitter, Reissner–Nordström and Kerr are analyzed with AIM. When you want to perform the analysis of QNM, this lead to a wave equation with a specific effective potential, depending on the characteristics of the effective potential some numerical methods are more suitable.

This paper is devoted to the study of the QNM and the time evolution of massless scalar and electromagnetic perturbations on Schwarzschild black hole with a deficit solid angle and quintessence-like matter. The wave-like perturbation equation, with an effective potential, can be solved to calculate the QNM numerically by two methods: the WKB approach (see [15–17]) and AIM (to demonstrate the viability of the method to obtain quasinormal modes). The paper is organized as follows: Section II we present the Black Hole considered in the present work and we briefly discuss the event horizons. In Sec. III we describe the scalar and electromagnetic perturbations of a Black Hole. We study the behavior of effective potential for different perturbations considering the special cases when the quintessence state parameter takes the values $-1/2$ and $-2/3$. In Sec. IV we present the results for quasinormal frequencies (QNFs) and in Sec.V we present the time domain analysis. Finally, our conclusions are in Sec. VI.

II. A SCHWARZSCHILD BLACK HOLE WITH QUINTESSENCE-LIKE MATTER AND A DEFICIT SOLID ANGLE

Barriola and Vilenkin [18] proposed static and spherical symmetric solution that describe Schwarzschild Black Hole with a deficit solid angle and quintessence-like matter. This solution is given by

$$ds^2 = f(r)dt^2 - \frac{dr^2}{f(r)} - r^2 d\theta^2 - r^2 \sin^2 \theta d\phi^2, \quad (1)$$

where

$$f(r) = 1 - \frac{2M}{r} - \epsilon^2 + \frac{\rho_0}{3\omega_0 r^{3\omega_0+1}}. \quad (2)$$

In which ϵ is the deficit solid angle parameter, ρ_0 is the density of quintessence-like matter, ω_0 is the quintessence state parameter and satisfies $-1 < \omega_0 < -1/3$ and M is the black hole mass. When $\epsilon = \rho_0 = 0$ the metric function $f(r)$ is reduced to the solution of Schwarzschild.

The horizons of Schwarzschild with quintessence-like matter and a deficit solid angle (Schwdm) are determined by the positive roots of the equation $f(r) = 0$, this condition leads to the polynomial

$$3\omega_0 (\epsilon^2 - 1) r^{3\omega_0+1} + 6M\omega_0 r^{3\omega_0} - \rho_0 = 0. \quad (3)$$

The number of horizons depends entirely on the choice of the values of parameters ϵ , ω_0 , M and ρ_0 . However, in an appropriated parametric region, the solution has two horizons: the event horizon r_+ and the cosmological horizon r_c . Using the ideas of [19], here hereafter, we fix the event horizon in $r_+ = 1$. To ensure $f(r_+) = 0$, it is required that the mass parameter can be expressed as

$$M = \frac{3\omega_0 (1 - \epsilon^2) + \rho_0}{6\omega_0}. \quad (4)$$

The region parametric in which the Schwdm BH has event horizon r_+ and cosmological horizon r_c are allowed, can be determined by $f'(r_+) > 0$. This condition leads to the next expression;

$$\rho_0 < 1 - \epsilon^2. \quad (5)$$

The region plot of the allowed parameter region is given in Fig. 1(a). For all values of (ϵ^2, ρ_0) in region shaded, there are two real positive roots of Eq. (3), $r_+ = 1$ and r_c , which satisfy $r_+ \leq r_c$. On the other hand, for values of $(\epsilon^2, \rho_0 = 1 - \epsilon^2)$ corresponding to the line represents extremal Schwdm BH, where $r_+ = r_c = 1$. In the Fig. 1(a) we observe that the parametric region is independent of ω_0 . From Fig. 1(b), we plot the metric function $f(r)$ for different values of ω_0 and we can conclude that the quintessence horizon is very large for $\omega_0 \rightarrow -1/3$.

Now inserting M (4) into (2), we can write the metric function as

$$f(r) = 1 - \epsilon^2 - \frac{1 - \epsilon^2 + \frac{\rho_0}{3\omega_0}}{r} + \frac{\rho_0}{3\omega_0 r^{3\omega_0+1}}. \quad (6)$$

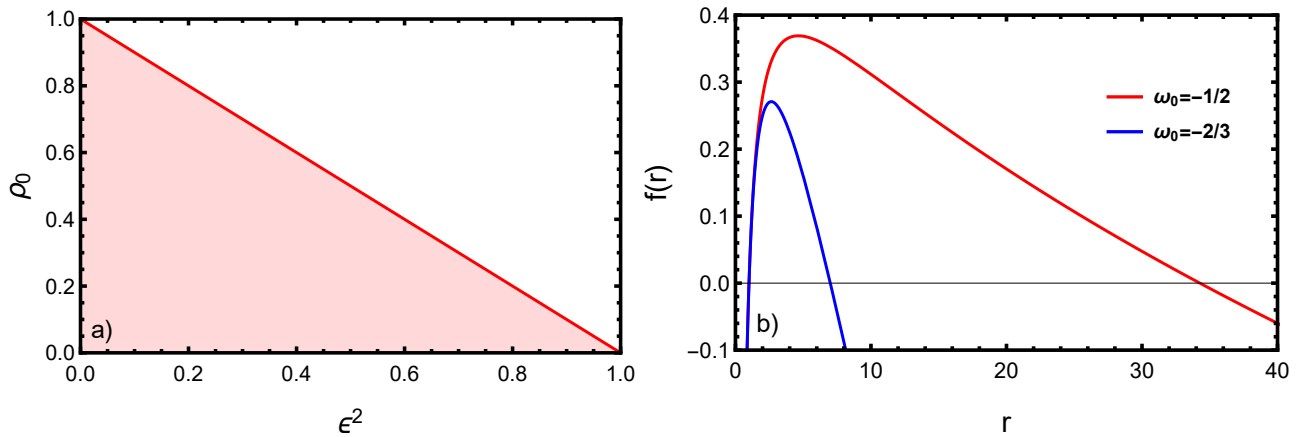


FIG. 1: a) The parametric region where the Schwdm BH has two horizons, $r_+ \leq r_c$ according to ω_0 values. The region is bounded by the line ($\rho_0 = 1 - \epsilon^2$), $\rho_0 = 0$ and $\epsilon = 0$ (the region shaded). b) The graph shows the metric function (2) as function of r for different values of ω_0 . Here $\rho_0 = 0.2$ and $\epsilon^2 = 0.2$.

For the particular case $\omega_0 = -2/3$, the cosmological and event horizons are given by

$$r_+ = 1, \quad r_c = \frac{2(1 - \epsilon^2) - \rho_0}{\rho_0}. \quad (7)$$

And for $\omega_0 = -1/2$, we get

$$r_+ = 1, \quad r_c = \frac{3[1 - \epsilon^2] - 2\rho_0}{2\rho_0} \left(1 + \frac{3[1 - \epsilon^2] - 2\rho_0 + \sqrt{3(3[1 - \epsilon^2] - 2\rho_0)(1 - \epsilon^2 + 2\rho_0)}}{4\rho_0} \right). \quad (8)$$

When the event and cosmological horizons coincide with each other, the Schwdm BH is an extremal one ($\rho_0 = 1 - \epsilon^2$), thus $r_+ = r_c = 1$.

To conclude this section, it is worth mentioning that if $r_+ \neq 1$ then expression (5) takes the following form

$$\rho_0 < (1 - \epsilon^2) \left[\frac{(1 - \epsilon^2)(3|\omega_0| - 1)}{6M|\omega_0|} \right]^{3|\omega_0| - 1}, \quad (9)$$

for further discussion, see the Ref. [11]. Which depends explicitly on ω_0 , so comparing the different parametric regions, it is possible to mention that the parametric region for $\omega_0 = -2/3$ is much smaller than the parametric region for $\omega_0 = -1/2$. It is worth mentioning that when we fix $r_+ = 1$, the parametric region (ϵ^2, ρ_0) (see Eq. (5) and Fig. 1) is independent of ω_0 , which facilitates the analysis of quasinormal modes.

III. SCALAR AND ELECTROMAGNETIC PERTURBATIONS

In this section, we briefly show the behavior of scalar and electromagnetic perturbations in a Black Hole with a deficit solid angle and quintessence-like matter, following the Refs. [16, 17]. The propagation of a scalar field in a curved background is described by the Klein-Gordon equation

$$\frac{1}{\sqrt{-g}} \partial_\mu (\sqrt{-g} g^{\mu\nu} \partial_\nu \Psi) = 0. \quad (10)$$

We separate variables by setting

$$\Psi(t, r, \theta, \phi) = \frac{1}{r} \phi(r) Y_{lm}(\theta, \phi) e^{i\omega t}, \quad (11)$$

where $Y_{lm}(\theta, \phi)$ are the spherical harmonics. Substituting Eq. (11) into (10), we get the next radial equation

$$\left[\frac{d^2}{dr_*^2} + \omega^2 - V_s(r) \right] \phi(r) = 0, \quad (12)$$

where r_* is the tortoise coordinate

$$dr_* = \frac{dr}{f(r)}, \quad (13)$$

and $V_s(r)$ is the effective potential

$$V_s(r) = f(r) \left[\frac{l(l+1)}{r^2} + \frac{f'(r)}{r} \right], \quad (14)$$

whereas, the electromagnetic field in curved space follows the next equation

$$\frac{1}{\sqrt{-g}} \partial_\mu (\sqrt{-g} F_{\beta\gamma} g^{\beta\nu} g^{\gamma\mu}) = 0, \quad (15)$$

where $F_{\beta\gamma} = \partial_\beta A_\gamma - \partial_\gamma A_\beta$ and the vector potential A_μ can be expressed as

$$A_0 = A_1 = A_2 = 0, \quad A_3 = \phi_e(r) \sin(\omega t) \sin \theta \frac{dP_l(\cos \theta)}{d\theta}. \quad (16)$$

After separation of variables, the radial parts of the electromagnetic field perturbation equation takes the form similar to (12), but the effective potential is given by

$$V_e(r) = f(r) \frac{l(l+1)}{r^2}. \quad (17)$$

From Eqs. (14) and (17), the scalar and electromagnetic perturbations can be described by a Schrödinger-like equation with potential

$$V(r) = f(r) \left[\frac{l(l+1)}{r^2} + (1-s) \frac{f'(r)}{r} \right], \quad (18)$$

where l is the multipole number ($l \geq s$), s is the spin of the perturbative field: $s = 0$ corresponding to scalar perturbation and $s = 1$ to electromagnetic perturbation. The effective potential (18) has asymptotic value $V(r) \approx \rho_0^2 (s-1)(1+s+3\omega_0) / (9\omega_0^2 r^{6\omega_0+4})$ when $r \rightarrow \infty$. From this behavior asymptotic for the effective potential, we can see that if $\omega_0 < -2/3$, $V \rightarrow \infty$ when $r \rightarrow \infty$. Thus we only study the case where the state parameter which has the range $-2/3 \leq \omega_0 < -1/3$. For the specific case $\omega_0 = -2/3$, the scalar perturbation, $V(r) \approx \rho_0^2/4$.

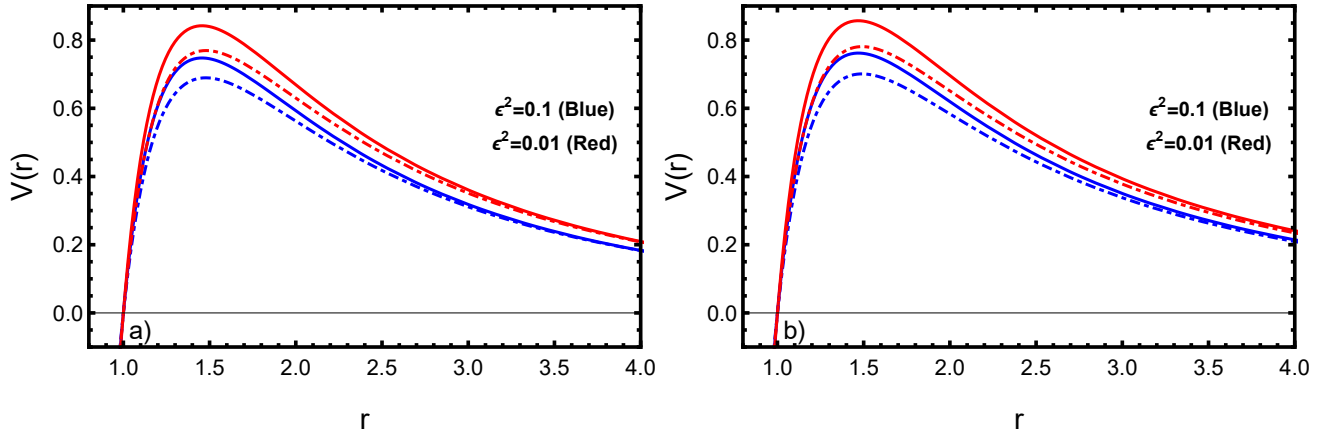


FIG. 2: a) The behavior of the effective potential for $\omega_q = -2/3$ is shown for various values of ϵ^2 , with $\rho_0 = 0.1$ and $l = 2$. b) The behavior of the effective potential for $\omega_q = -1/2$ is shown for various values of ϵ^2 , with $\rho_0 = 0.1$ and $l = 2$. In both figures, the effective potential of scalar (solid) and electromagnetic (dot dashed)

The behavior of $V(r)$ for different values of ϵ^2 is described in Fig. 2 a) and b) for $\omega_q = -2/3$ and $\omega_q = -1/2$ respectively, while the behavior of effective potential for different values of ρ_0 is described in Fig. 3 for different values of state parameter. Furthermore, the form of the effective potential is very similar to that obtained in the quintessence case for scalar and fermionic perturbations [20].

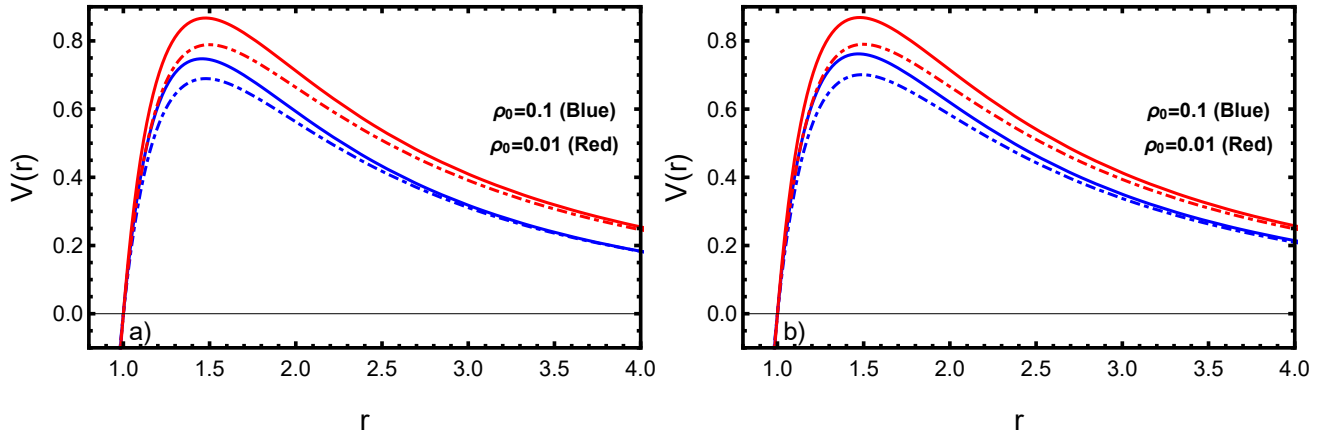


FIG. 3: a) The behavior of the effective potential for $\omega_q = -2/3$ is shown for various values of ρ_0 , with $\epsilon^2 = 0.1$ and $l = 2$. b) The behavior of the effective potential for $\omega_q = -1/2$ is shown for various values of ρ_0 , with $\epsilon^2 = 0.1$ and $l = 2$. In both figures, the effective potential of scalar (solid) and electromagnetic (dot dashed)

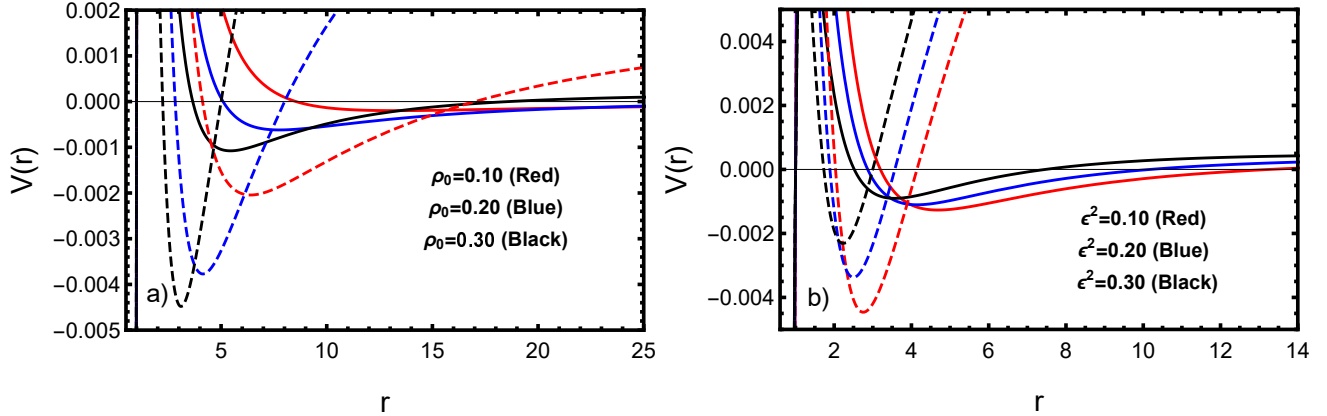


FIG. 4: The effective potential of scalar field with $l = 0$ mode. The a) and b) plots correspond to $\epsilon^2 = 0.1$ and $\rho = 0.35$ respectively. In both figures, the effective potential for $\omega_0 = -1/2$ is represented by the solid line and by the dotted line for $\omega_0 = -2/3$.

It is worth mentioning that the effective potential is positive definite for $r_* \in [-\infty, \infty]$ and have a potential barrier near the event horizon for very small values of the state parameter and deficit solid angle parameter.

From Figs. 2 and 3 we can mention that in both cases $V_{elec}(r) < V_{sc}(r)$.

If we study the effective potential for scalar field with $l = 0$ mode, we can see that $V(r)$ can take negative values between r_+ and r_c (see Figs. 4(a) and 4(b)). This potential well is the key point for the occurrence of instability. However, the negative effective potential does not guarantee that the imaginary part of the quasinormal frequencies takes positive values i.e. the existence of a negative potential well can be viewed as the necessary but not sufficient condition for instability [21].

Also we can see in Fig. 4(a) that for increasing values of ρ_0 , the depth of the potential well increases, while in Fig. 4(b) shows that for increasing values of ϵ^2 , the depth of the potential well decreases. The stability or instability analysis of scalar perturbations for the case $l = 0$, is discussed in Sec. V.

The Eq. (12) exhibits the following behavior near the horizons

$$\phi_s \approx \begin{cases} e^{-i\omega r_*}, & r_* \rightarrow -\infty (r \rightarrow r_+) \\ e^{i\omega r_*}, & r_* \rightarrow \infty (r \rightarrow r_c) \end{cases}, \quad (19)$$

the asymptotic solutions (19) imply that the wave at the event horizon is purely incoming, whereas at the cosmological horizon is purely outgoing. For the boundary condition mentioned above, the wave equation (12) can be solved in order to obtain the spectrum of the quasi normal frequencies.

IV. QNM: IMPROVED ASYMPTOTIC ITERATION METHOD

It is well known that in the literature, there are some numerical and semianalytical methods to calculate QNM. The method suggested by Mashhoon [22], where the potential barrier in the Schrödinger-like equation is replaced by a potential barrier for which we know the analytic solution. This method gives quite accurate results for the regime of high multipole numbers. Besides the method by Leaver [23], typically by applying a Frobenius series solution approach, leading to continued fractions for QNM. Another technique is the WKB approximation (this approach has been extended to the sixth order, see [24]), this approach gives more accuracy and can be carried to a higher order. However, the WKB approach does not give reliable frequencies for $n \geq l$. As mentioned, these techniques have some limitations. On the other hand, another new method that has been developed that may be more efficient in some cases is the asymptotic iteration method.

The AIM has been used to calculate the QNM of black holes in the asymptotic dS spacetimes [14, 25] To apply AIM, we need to introducing the transformation of coordinates $\xi = 1/r$. In the new coordinate ξ , the equation (12), which leads to the following expression

$$\left[\frac{d^2}{d\xi^2} + \frac{p'}{p} \frac{d}{d\xi} + \frac{\omega^2}{p^2} - \frac{l(l+1) + (1-s^2) \left(1 - \epsilon^2 - \frac{p}{\xi^2}\right) - (1-s) \rho_0 \xi^{3\omega_0+1}}{p} \right] \phi = 0, \quad (20)$$

where the prime denotes derivative with respect ξ , and $p(\xi)$ is defined as

$$p(\xi) = (1 - \epsilon^2) \xi^2 - \frac{3\omega_0 (1 - \epsilon^2) + \rho_0}{3\omega_0} \xi^3 + \frac{\rho_0}{3\omega_0} \xi^{3(\omega_0+1)}. \quad (21)$$

To accommodate the outgoing wave boundary condition $\phi \rightarrow e^{i\omega r_*}$ in terms of ξ , we define

$$e^{i\omega r_*} = e^{-i\omega \int \frac{d\xi}{p(\xi)}}. \quad (22)$$

The expression (22) scale out the divergence behavior at the cosmological horizon. So, by implement the boundary conditions in the AIM, we redefine the function ϕ in terms of the new function χ . So we can write

$$\phi(\xi) = e^{-i\omega \int \frac{d\xi}{p(\xi)}} (\xi - \xi_+)^{-i\omega/\kappa_+} \chi(\xi). \quad (23)$$

Considering (23), we can scale out the divergent behavior at the event horizon. Here κ_+ is the surface gravity at the horizon defined as;

$$\kappa_+ = \frac{1}{2} \frac{d}{dr} f(r) \Big|_{r \rightarrow r_+} = - \frac{\xi^2}{2} \frac{d}{d\xi} f(\xi) \Big|_{\xi \rightarrow \xi_+}. \quad (24)$$

By combining equations (20) and (23), we obtain the following differential equation for $\chi(\xi)$

$$\frac{d^2 \chi(\xi)}{d\xi^2} = \lambda_0(\xi) \frac{d\chi(\xi)}{d\xi} + s_0(\xi) \chi(\xi), \quad (25)$$

where

$$\lambda_0(\xi) = \frac{2i\omega}{\kappa_+(\xi - \xi_+)} - \frac{p' - 2i\omega}{p}, \quad (26)$$

$$s_0(\xi) = \frac{l(l+1) + (1-s) \left(1 - \epsilon^2 - \frac{p}{\xi^2} - \rho_0 \xi^{3\omega_0+1}\right)}{p} - \frac{i\omega(\kappa_+ + i\omega)}{\kappa_+^2 (\xi - \xi_+)^2} + \frac{i\omega(p' - 2i\omega)}{p\kappa_+(\xi - \xi_+)}. \quad (27)$$

Now following the improved AIM procedure, the expressions (26) and (27) are used in the relations (A.6) and (A.7) (see Appendix) to calculate the quantities that appear in the quantization condition (A.10). The stable roots of condition (A.10) are the QNM of the scalar and electromagnetic test fields. We use Mathematica Software to perform all the calculations.

We present in Tables I, II, III and IV results for scalar and electromagnetical perturbation respectively. We compared our results obtained using AIM (after of fifteen iterations) with WKB to sixth-order. From Tables I-IV, we can see that between the WKB method and AIM, there are differences in the values of QNM at $n = l = 0$, (it is well

Scalar perturbations				
$\omega_0 = -2/3$		$\omega_0 = -1/2$		
	WKB	AIM	WKB	AIM
ϵ^2				
			$l = 0$	
0.01	0.187043-0.191982 <i>i</i>	0.186947-0.195326 <i>i</i>	0.190396-0.184349 <i>i</i>	0.190432-0.189805 <i>i</i>
0.10	0.166671-0.174322 <i>i</i>	0.167064-0.176485 <i>i</i>	0.170528-0.166209 <i>i</i>	0.170589-0.170975 <i>i</i>
ϵ^2			$l = 1$	
0.01	0.536367-0.175563 <i>i</i>	0.536404-0.175406 <i>i</i>	0.542744-0.174016 <i>i</i>	0.542784-0.173865 <i>i</i>
0.10	0.504477-0.15763 <i>i</i>	0.504505-0.157515 <i>i</i>	0.510936-0.156189 <i>i</i>	0.510967-0.156078 <i>i</i>
			$l = 3$	
0.01	1.252810-0.172128 <i>i</i>	1.252810-0.172127 <i>i</i>	1.263260-0.171518 <i>i</i>	1.263260-0.171517 <i>i</i>
0.10	1.184560-0.154697 <i>i</i>	1.184560-0.154696 <i>i</i>	1.195430-0.154106 <i>i</i>	1.195430-0.154105 <i>i</i>
			$l = 5$	
0.01	1.969140-0.171672 <i>i</i>	1.969140-0.171672 <i>i</i>	1.984550-0.171193 <i>i</i>	1.984550-0.171193 <i>i</i>
0.10	1.863150-0.154311 <i>i</i>	1.863150-0.154311 <i>i</i>	1.879280-0.153837 <i>i</i>	1.879280-0.153837 <i>i</i>
			$l = 7$	
0.01	2.685400-0.171528 <i>i</i>	2.685400-0.171528 <i>i</i>	2.705960-0.171091 <i>i</i>	2.705960-0.171091 <i>i</i>
0.10	2.541410-0.154190 <i>i</i>	2.541410-0.154190 <i>i</i>	2.562970-0.153753 <i>i</i>	2.562970-0.153753 <i>i</i>

TABLE I: Quasinormal frequencies for the Scalar perturbations for several values of the parameter ϵ^2 , with $n = 0$ and $\rho_0 = 0.1$.

Scalar perturbations				
$\omega_0 = -2/3$		$\omega_0 = -1/2$		
	WKB	AIM	WKB	AIM
ρ_0				
			$l = 0$	
0.01	0.195563-0.180831 <i>i</i>	0.195457-0.187169 <i>i</i>	0.195975-0.179954 <i>i</i>	0.195743-0.186603 <i>i</i>
0.10	0.166671-0.174322 <i>i</i>	0.167064-0.176485 <i>i</i>	0.170528-0.166209 <i>i</i>	0.170589-0.170975 <i>i</i>
ρ_0			$l = 1$	
0.01	0.547237-0.173928 <i>i</i>	0.547278-0.173778 <i>i</i>	0.547896-0.173768 <i>i</i>	0.547937-0.173619 <i>i</i>
0.10	0.504477-0.157630 <i>i</i>	0.504505-0.157515 <i>i</i>	0.510936-0.156189 <i>i</i>	0.510967-0.156078 <i>i</i>
			$l = 3$	
0.01	1.270480-0.171755 <i>i</i>	1.270480-0.171753 <i>i</i>	1.271550-0.171696 <i>i</i>	1.271550-0.171695 <i>i</i>
0.10	1.184560-0.154697 <i>i</i>	1.184560-0.154696 <i>i</i>	1.195430-0.154106 <i>i</i>	1.195430-0.154105 <i>i</i>
			$l = 5$	
0.01	1.995190-0.171473 <i>i</i>	1.995190-0.171473 <i>i</i>	1.996760-0.171429 <i>i</i>	1.996760-0.171429 <i>i</i>
0.10	1.863150-0.154311 <i>i</i>	1.863150-0.154311 <i>i</i>	1.879280-0.153837 <i>i</i>	1.879280-0.153837 <i>i</i>
			$l = 7$	
0.01	2.720170-0.171385 <i>i</i>	2.720170-0.171385 <i>i</i>	2.722270-0.171345 <i>i</i>	2.722270-0.171345 <i>i</i>
0.10	2.541410-0.154190 <i>i</i>	2.541410-0.154190 <i>i</i>	2.562970-0.153753 <i>i</i>	2.562970-0.153753 <i>i</i>

TABLE II: Quasinormal frequencies for the Scalar perturbations for several values of the parameter ρ_0 , with $n = 0$ and $\epsilon^2 = 0.1$.

known that WKB approximation does not give reliable frequencies for $n \geq l$) and the case for higher l the differences are smaller between both methods.

In Table I and Table III, we can observe the frequencies of the QNM for the scalar and electromagnetic perturbations, the real part increases when l increases and we fix the parameter ρ_0 . The same behavior occurs when the parameter ϵ is fixed (see Tables II and IV). In the cases of the imaginary part when the parameters ρ_0 or ϵ are fixed, their values increase as l increases, for both perturbations, then we can mention that the relaxation time of the Schwdm BH diminishes and the BH is stable.

An interesting feature, we noticed is that due to quintessence-like matter, the scalar and electromagnetic fields damp more rapidly when the parameter ω_0 increases. Tables I-IV show as the parameter ω_0 increases, the magnitudes of the real part of the frequencies of the QNM increase. In contrast, the absolute value of the imaginary part of the frequencies of the QNM decreases. On the other hand, comparing our results presented in this work with those that use the Kiselev model, the scalar field also decays more rapidly for higher values of state parameter in the case of Schwarzschild surrounded by quintessence, as shown in Ref. [10]. In this reference, the state parameter plays the same role as the parameter ω_0 in our case.

It can be seen that the range of real and imaginary frequencies is approximately the same and it does not change drastically when the WKB or the AIM are considered, so the AIM is very reliable because in this case few iterations

Electromagnetic perturbations				
	$\omega_0 = -2/3$		$\omega_0 = -1/2$	
	WKB	AIM	WKB	AIM
ϵ^2				
			$l = 1$	
0.01	0.465629-0.165506 <i>i</i>	0.465727-0.165296 <i>i</i>	0.469719-0.165173 <i>i</i>	0.469814-0.164968 <i>i</i>
0.10	0.444590-0.149292 <i>i</i>	0.444653-0.149151 <i>i</i>	0.448856-0.148948 <i>i</i>	0.448918-0.148810 <i>i</i>
			$l = 3$	
0.01	1.223820-0.170371 <i>i</i>	1.223820-0.170370 <i>i</i>	1.233200-0.169992 <i>i</i>	1.233200-0.169991 <i>i</i>
0.10	1.160040-0.153247 <i>i</i>	1.160040-0.153246 <i>i</i>	1.169890-0.152861 <i>i</i>	1.169890-0.152860 <i>i</i>
			$l = 5$	
0.01	1.950800-0.170964 <i>i</i>	1.950800-0.170964 <i>i</i>	1.965510-0.170580 <i>i</i>	1.965510-0.170580 <i>i</i>
0.10	1.847640-0.153727 <i>i</i>	1.847640-0.153727 <i>i</i>	1.863110-0.153337 <i>i</i>	1.879280-0.153837 <i>i</i>
			$l = 7$	
0.01	2.671970-0.171148 <i>i</i>	2.671970-0.171148 <i>i</i>	2.692020-0.170762 <i>i</i>	2.692020-0.170762 <i>i</i>
0.10	2.530050-0.153876 <i>i</i>	2.530050-0.153876 <i>i</i>	2.551140-0.153484 <i>i</i>	2.551140-0.153484 <i>i</i>

TABLE III: Quasinormal frequencies for the Electromagnetic perturbations for several values of the parameter ϵ , with $n = 0$ and $\rho_0 = 0.1$.

Electromagnetic perturbations				
	$\omega_0 = -2/3$		$\omega_0 = -1/2$	
	WKB	AIM	WKB	AIM
ρ_0				
			$l = 1$	
0.01	0.472513-0.165563 <i>i</i>	0.472604-0.165367 <i>i</i>	0.472932-0.165534 <i>i</i>	0.473022-0.165339 <i>i</i>
0.10	0.444590-0.149292 <i>i</i>	0.444653-0.149151 <i>i</i>	0.448856-0.148948 <i>i</i>	0.448918-0.148810 <i>i</i>
			$l = 3$	
0.01	1.239670-0.170316 <i>i</i>	1.239670-0.170314 <i>i</i>	1.240630-0.170282 <i>i</i>	1.240630-0.170281 <i>i</i>
0.10	1.160040-0.153247 <i>i</i>	1.160040-0.153246 <i>i</i>	1.169890-0.152861 <i>i</i>	1.169890-0.152860 <i>i</i>
			$l = 5$	
0.01	1.975680-0.170895 <i>i</i>	1.975680-0.170895 <i>i</i>	1.977180-0.170861 <i>i</i>	1.977180-0.170861 <i>i</i>
0.10	1.847640-0.153727 <i>i</i>	1.847640-0.153727 <i>i</i>	1.863110-0.153337 <i>i</i>	1.863110-0.153337 <i>i</i>
			$l = 7$	
0.01	2.705880-0.171074 <i>i</i>	2.705880-0.171074 <i>i</i>	2.707920-0.171041 <i>i</i>	2.707920-0.171041 <i>i</i>
0.10	2.530050-0.153876 <i>i</i>	2.530050-0.153876 <i>i</i>	2.551140-0.153484 <i>i</i>	2.551140-0.153484 <i>i</i>

TABLE IV: Quasinormal frequencies for the Electromagnetic perturbations for several values of the parameter ρ_0 , with $n = 0$ and $\epsilon^2 = 0.1$.

are required to compute the quasinormal modes. On the other hand, the calculation time is much less compared to WKB. This feature can be useful to study another more complicated black hole solution.

V. TIME EVOLUTION OF SCALAR AND ELECTROMAGNETIC PERTURBATIONS

In this section we compute the time evolution of the Scalar and Electromagnetic perturbations to further reveal the instability of the Schwarzschild black hole with quintessence-like matter and a deficit solid angle. For the time evolution, the radial part of the perturbation equations are reduced to the form

$$\frac{\partial^2 \Psi}{\partial t^2} - \frac{\partial^2 \Psi}{\partial r_*^2} + V(r)\Psi = 0. \quad (28)$$

After recasting the wave equation (28) in the null coordinates $u = t - r_*$ and $v = t + r_*$ we obtain

$$-4 \frac{\partial^2}{\partial u \partial v} \Psi(u, v) = V(u, v)\Psi(u, v). \quad (29)$$

In order to compute the time evolution of Ψ we implemented the discretization scheme developed in [26], i.e. we can numerically integrate by using the finite difference method. Using the Taylor expansion, one find

$$\begin{aligned} \Psi(u + \Delta u, v + \Delta v) &= \Psi(u, v + \Delta v) + \Psi(u + \Delta u, v) - \Psi(u, v) \\ &\quad - \frac{\Delta u \Delta v}{8} V \left(\frac{2v - 2u + \Delta v - \Delta u}{4} \right) [\Psi(u + \Delta u, v) + \Psi(u, v + \Delta v)] + O(h^4), \end{aligned} \quad (30)$$

where h is an overall grid scalar factor ($\Delta u = \Delta v = h$). To perform the numerical integration on an uniformly spaced grid. we impose the following initial profile

$$\Psi(u, v = 0) = 0, \quad \psi(u = 0, v) = Ae^{-\frac{(v-v_0)^2}{2\sigma^2}}, \quad (31)$$

since the late-time behavior of the wave function is found to be insensitive to the initial data, we set the initial Gaussian distribution with width, $\sigma = 3$ centered at $v_0 = 10$, amplitude $A = 1$ and with an overall grid scale factor $h = 0.2$. To proceed the integration in the aforementioned scheme one has to find the value of the potential at $r(r_*)$ at each step.

For the special case $\omega_0 = -2/3$, we get

$$r_* = \frac{1}{2\kappa_+} \ln \left| \frac{r}{r_+} - 1 \right| + \frac{1}{2\kappa_c} \ln \left| 1 - \frac{r}{r_c} \right|, \quad (32)$$

and for $\omega_0 = -1/2$, we obtain

$$r_* = -\frac{3\sqrt{r}}{\rho_0} - \frac{1}{2\kappa_+} \ln \left| \frac{\sqrt{r}}{r_+} - 1 \right| - \frac{3r_1^3}{\rho_0(r_1 - 1)(r_1 - r_2)} \ln \left| 1 - \frac{\sqrt{r}}{r_1} \right| + \frac{3r_2^3}{\rho_0(r_2 - 1)(r_1 - r_2)} \ln \left| 1 - \frac{\sqrt{r}}{r_2} \right|, \quad (33)$$

where

$$r_{1,2} = \frac{1}{4\rho_0} \left[3(1 - \epsilon^2) - 2\rho_0 \pm \sqrt{3[3(1 - \epsilon^2) - 2\rho_0][1 - \epsilon^2 + 2\rho_0]} \right]. \quad (34)$$

So we get $r(r_*)$ numerically, using the built-in Mathematica commands.

In Fig. 5 we show the evolution profile of the scalar field for $l = 0$ mode. We observe that the $\text{Log}|\Psi|$ linearly depends on t at later times. From Fig. 5(a) we see that the perturbations start to become unstable for higher values of ρ_0 , whereas if the values of ϵ^2 increases, the system becomes stable. In both graphs when the value of the quintessence parameter ω_0 increases, the system becomes more stable, which is in correspondence with the peculiar shape of the potential for $\omega_0 = -2/3$ and $\omega_0 = -1/2$ (Fig. 4).

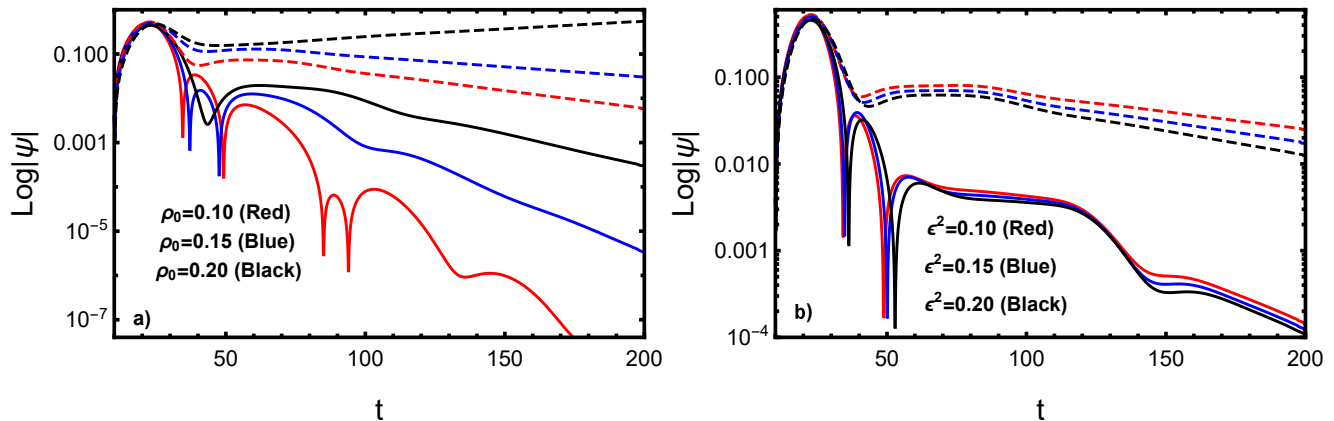


FIG. 5: Logarithmic plot of the evolution of a scalar field in Schwdm BH for the case of $l = 0$ mode. a) the plot correspond to $\epsilon = 0.1$ and b) the plot correspond to $\rho_0 = 0.1$. In both graphs, the solid line is for $\omega_0 = -1/2$, while the dotted line is for $\omega_0 = -2/3$.

Fig. 6 demonstrates the evolution of scalar field around of the Schwdm BH with different ρ_0 , ϵ^2 and ω_0 , and in the Fig. 7 the evolution of electromagnetic field is showed.

One can see from Fig. 6 and Fig. 7 that difference of the temporal evolution of the perturbations in the Schwdm BH, is that increases the frequencies of oscillation in the case of the electromagnetic perturbation. Also, it is possible to notice that at $\omega_0 = -1/2$ and $\omega_0 = -2/3$ of the Schwdm BH, the evolution of the perturbations are almost the same. Moreover, time domain profiles of the scalar and electromagnetic perturbations of the black hole show that it is stable against perturbations.

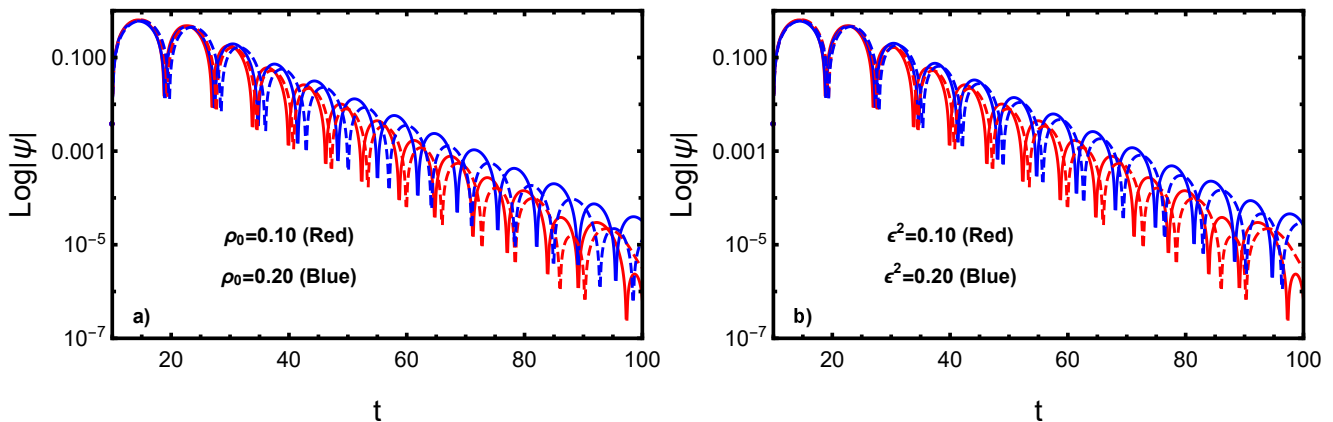


FIG. 6: Logarithmic plot of the evolution of a scalar field in Schwdm BH for the case of $l = 1$ mode. a) the plot correspond to $\epsilon = 0.1$ and b) the plot correspond to $\rho_0 = 0.1$. In both graphs, the solid line is for $\omega_0 = -1/2$, while the dotted line is for $\omega_0 = -2/3$.

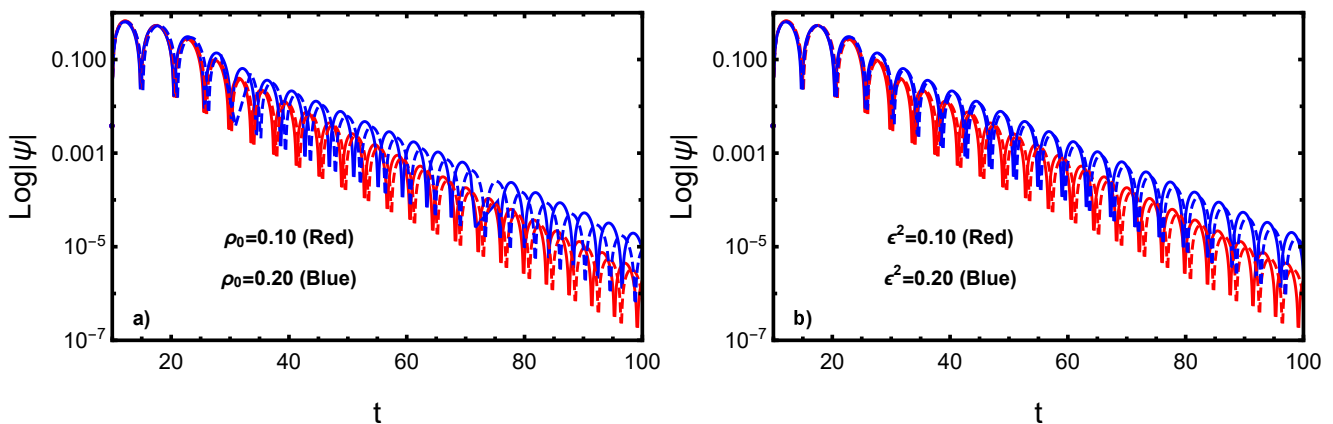


FIG. 7: Logarithmic plot of the evolution of a electromagnetic field in Schwdm BH for the case of $l = 2$ mode. a) the plot correspond to $\epsilon = 0.1$ and b) the plot correspond to $\rho_0 = 0.1$. In both graphs, the solid line is for $\omega_0 = -1/2$, while the dotted line is for $\omega_0 = -2/3$.

VI. CONCLUSIONS

In this contribution, we have focused on scalar and electromagnetic perturbations of spherically symmetric Schwarzschild black hole with quintessence-like matter and a deficit solid angle. First, we numerically calculated the real and imaginary frequencies of the QNM. Secondly, we studied the time evaluation of scalar and electromagnetic perturbations.

We calculated the QNM of Schwdm BH, we apply mainly the improved AIM and WKB approximation sixth order to make a comparison between both methods. The magnitudes of the real part and the imaginary part of the QNM for scalar and electromagnetic perturbations decrease with the decreases of values of the density of quintessence-like matter and deficit solid angle. The frequencies are approximately the same and it does not change drastically when the WKB method or the AIM are considered, so AIM is very reliable, in this particular case, because few iterations are required to compute the quasinormal modes also the calculation time is much less compared to WKB.

From Tables I-IV, we can see that the change with respect to ω_0 of the real part and the magnitude of the imaginary part of the frequencies is very small, while the real part increase with increasing l and the increase of the magnitude of imaginary part of the frequencies is very small.

The evolution of scalar and electromagnetic perturbations obtained in this work confirms that in the QNM stage, all the fields decay slowly due to the presence of quintessence-like matter. At late times, the frequencies are suppressed by the tail form of field decay. However, from Fig. 5(a), we can see that the late decay of scalar perturbations with $l = 0$ gives up the power law form of decay, relaxing to a constant field. This constant value of the field increases as the values of ρ_0 increase, while it decreases if the values of ϵ increase (This behavior can be understood as a consequence

of cosmological no-hair theorem).

We also saw the behavior of perturbations with changing parameter ρ_0 , ϵ^2 and ω_0 . We note that perturbations with the higher value of ρ_0 becomes unstable for the $l = 0$ mode of the scalar field. The behavior of the perturbation for different values of the ϵ^2 and ω_0 is also studied and reported.

In general, we also observed that the different parameters have a critical role in black hole stability. The results obtained for QNM frequencies can play a significant role as an indirect way of detecting dark energy near the black hole by using future gravitational wave detectors for interactions of scalar fields with the black hole.

Appendix: Improved AIM

In this appendix we briefly explain the improved AIM. We shall start with the second-order differential equation for the function $\chi(\xi)$

$$\chi'' = \lambda_0(\xi)\chi' + s_0(\xi)\chi. \quad (\text{A.1})$$

We can express higher derivatives of $\chi(\xi)$ in terms of $\chi'(\xi)$ and $\chi(\xi)$, as following

$$\chi^{(n+2)} = \lambda_n(\xi)\chi' + s_n(\xi)\chi, \quad (\text{A.2})$$

where

$$\lambda_n(\xi) = \lambda'_{n-1}(\xi) + s_{n-1}(\xi) + \lambda_0(\xi)\lambda_{n-1}(\xi), \quad (\text{A.3})$$

$$s_n(\xi) = s'_{n-1}(\xi) + s_0(\xi)\lambda_{n-1}(\xi). \quad (\text{A.4})$$

For sufficiently large n , the coefficients $\lambda_n(\xi)$ and $s_n(\xi)$ satisfy the quantization relation

$$s_n\lambda_{n-1} - s_{n-1}\lambda_n = 0. \quad (\text{A.5})$$

Here, the eigenvalues are given by roots of (A.5). However, for each iteration, we must take derivatives of λ_{n-1} and s_{n-1} to compute λ_n and s_n , so this process can slow the numerical implementation of the AIM down considerably and it can increase execution time. To overcome this issues, an improved version of AIM was developed in Ref. [25], which avoids the need to take derivatives at each step.

Now, expand the $\lambda_n(\xi)$ and $s_n(\xi)$ in a Taylor series around the point ξ_0 , we have

$$\lambda_n(\xi) = \sum_{i=0}^{\infty} c_n^i (\xi - \xi_0)^i, \quad (\text{A.6})$$

$$s_n(\xi) = \sum_{i=0}^{\infty} d_n^i (\xi - \xi_0)^i, \quad (\text{A.7})$$

where c_n^i and d_n^i are the i th Taylor coefficients. Substituting (A.6) and (A.7) in (A.3) and (A.4), we have the following recursion relations for the coefficients

$$c_n^i = (i+1)c_{n-1}^{i+1} + d_{n-1}^i + \sum_{j=0}^i c_0^j c_{n-1}^{i-j}, \quad (\text{A.8})$$

$$d_n^i = (i+1)d_{n-1}^{i+1} + \sum_{j=0}^i d_0^j c_{n-1}^{i-j}, \quad (\text{A.9})$$

then, the quantization condition (A.5) can be rewritten as

$$d_n^0 c_{n-1}^0 - d_{n-1}^0 c_n^0 = 0. \quad (\text{A.10})$$

Using the quantization condition (A.10) we can obtain QNM, for n large enough.

ACKNOWLEDGMENT

The authors acknowledge the partial financial support from SNII–CONAHCYT, México.

-
- [1] Sai Iyer. BLACK HOLE NORMAL MODES: A WKB APPROACH. 2. SCHWARZSCHILD BLACK HOLES. *Phys. Rev. D*, 35:3632, 1987.
 - [2] Kai Lin, Jin Li, and Shuzheng Yang. Quasinormal Modes of Hayward Regular Black Hole. *Int. J. Theor. Phys.*, 52:3771–3778, 2013.
 - [3] Sharmanthie Fernando and Juan Correa. Quasinormal Modes of Bardeen Black Hole: Scalar Perturbations. *Phys. Rev. D*, 86:064039, 2012.
 - [4] Chong Oh Lee, Jin Young Kim, and Mu-In Park. Quasi-normal modes and stability of Einstein–Born–Infeld black holes in de Sitter space. *Eur. Phys. J. C*, 80(8):763, 2020.
 - [5] L. A. López and Valeria Ramírez. Quasi-normal modes of a Generic-class of magnetically charged regular black hole: scalar and electromagnetic perturbations. *Eur. Phys. J. Plus*, 138(2):120, 2023.
 - [6] Omar Pedraza, L. A. López, R. Arceo, and I. Cabrera-Munguia. Quasinormal modes of the Hayward black hole surrounded by quintessence: Scalar, electromagnetic and gravitational perturbations. *Mod. Phys. Lett. A*, 37(09):2250057, 2022.
 - [7] Mahamat Saleh, Bouetou Thomas Bouetou, and Timoleon Crepin Kofane. Quasinormal modes and Hawking radiation of a Reissner–Nordstrom black hole surrounded by quintessence. *Astrophys. Space Sci.*, 333:449–455, 2011.
 - [8] V. V. Kiselev. Quintessence and black holes. *Class. Quant. Grav.*, 20:1187–1198, 2003.
 - [9] Y. Zhang and Y. X. Gui. Quasinormal modes of a Schwarzschild black hole surrounded by quintessence. *Class. Quant. Grav.*, 23:6141–6147, 2006.
 - [10] Song-bai Chen and Ji-liang Jing. Quasinormal modes of a black hole surrounded by quintessence. *Class. Quant. Grav.*, 22:4651–4657, 2005.
 - [11] Chengye Yu, Deyou Chen, and Chuanhong Gao. Quasinormal modes and the correspondence with shadow in black holes with a deficit solid angle and quintessence-like matter. *Nucl. Phys. B*, 983:115925, 2022.
 - [12] B. Hamil and B. C. Lütfüoğlu. Noncommutative Schwarzschild black hole surrounded by quintessence: Thermodynamics, Shadows and Quasinormal modes. *Phys. Dark Univ.*, 44:101484, 2024.
 - [13] Hakan Ciftci, Richard L Hall, and Nasser Saad. Asymptotic iteration method for eigenvalue problems. *Journal of Physics A: Mathematical and General*, 36(47):11807, nov 2003.
 - [14] H. T. Cho, A. S. Cornell, Jason Doukas, T. R. Huang, and Wade Naylor. A New Approach to Black Hole Quasinormal Modes: A Review of the Asymptotic Iteration Method. *Adv. Math. Phys.*, 2012:281705, 2012.
 - [15] Ping Xi. Quasinormal modes of a black hole with quintessence-like matter and a deficit solid angle. *Astrophys. Space Sci.*, 321:47–51, 2009.
 - [16] Ping Xi, Xi-chen Ao, and Xin-zhou Li. A Simple derivation of level spacing of quasinormal frequencies for a black hole with a deficit solid angle and quintessence-like matter. *Astrophys. Space Sci.*, 330:273–278, 2010.
 - [17] Chun-Yan Wang, Ya-Feng Zhao, and Ya-Jun Gao. Quasinormal Modes of a Black Hole with Quintessence-Like Matter and a Deficit Solid Angle for Electromagnetic Perturbation. *Commun. Theor. Phys.*, 57(6):1101–1104, 2012.
 - [18] Manuel Barriola and Alexander Vilenkin. Gravitational Field of a Global Monopole. *Phys. Rev. Lett.*, 63:341, 1989.
 - [19] Peng Liu, Chao Niu, and Cheng-Yong Zhang. Instability of regularized 4D charged Einstein–Gauss–Bonnet de-Sitter black holes. *Chin. Phys. C*, 45(2):025104, 2021.
 - [20] Ahmad Al-Badawi, İzzet Sakallı, and Sara Kanzi. Solution of dirac equation and greybody radiation around a regular bardeen black hole surrounded by quintessence. *Annals of Physics*, 412:168026, 2020.
 - [21] K. A. Bronnikov, R. A. Konoplya, and A. Zhidenko. Instabilities of wormholes and regular black holes supported by a phantom scalar field. *Phys. Rev. D*, 86:024028, Jul 2012.
 - [22] Hans-Joachim Blome and Bahram Mashhoon. Quasi-normal oscillations of a schwarzschild black hole. *Physics Letters A*, 100(5):231–234, 1984.
 - [23] E. W. Leaver. An Analytic representation for the quasi normal modes of Kerr black holes. *Proc. Roy. Soc. Lond. A*, 402:285–298, 1985.
 - [24] RA Konoplya. Quasinormal behavior of the d-dimensional schwarzschild black hole and the higher order wkb approach. *Physical Review D*, 68(2):024018, 2003.
 - [25] H. T. Cho, A. S. Cornell, Jason Doukas, and Wade Naylor. Black hole quasinormal modes using the asymptotic iteration method. *Class. Quant. Grav.*, 27:155004, 2010.
 - [26] Carsten Gundlach, Richard H. Price, and Jorge Pullin. Late time behavior of stellar collapse and explosions: 1. Linearized perturbations. *Phys. Rev. D*, 49:883–889, 1994.